



HAL
open science

The effects of the pre-reversal ExB drift, the EIA asymmetry, and magnetic activity on the equatorial spread F during solar maximum

C.-C. Lee, J.-Y. Liu, B. W. Reinisch, W.-S. Chen, F.-D. Chu

► **To cite this version:**

C.-C. Lee, J.-Y. Liu, B. W. Reinisch, W.-S. Chen, F.-D. Chu. The effects of the pre-reversal ExB drift, the EIA asymmetry, and magnetic activity on the equatorial spread F during solar maximum. *Annales Geophysicae*, 2005, 23 (3), pp.745-751. hal-00317603

HAL Id: hal-00317603

<https://hal.science/hal-00317603>

Submitted on 18 Jun 2008

HAL is a multi-disciplinary open access archive for the deposit and dissemination of scientific research documents, whether they are published or not. The documents may come from teaching and research institutions in France or abroad, or from public or private research centers.

L'archive ouverte pluridisciplinaire **HAL**, est destinée au dépôt et à la diffusion de documents scientifiques de niveau recherche, publiés ou non, émanant des établissements d'enseignement et de recherche français ou étrangers, des laboratoires publics ou privés.

The effects of the pre-reversal drift, the EIA asymmetry, and magnetic activity on the equatorial spread F during solar maximum

C.-C. Lee¹, J.-Y. Liu², B. W. Reinisch³, W.-S. Chen², and F.-D. Chu^{2,4}

¹General Education Center, Ching-Yun University, No. 229, Chienshin Road, Zhongli City, Taoyuan County 320, Taiwan

²Institute of Space Science, National Central University, No. 300, Zhongda Rd., Zhongli City, Taoyuan County 320, Taiwan

³Center for Atmospheric Research, University of Massachusetts Lowell, 600 Suffolk Street, Lowell, MA 01854, USA

⁴National Standard Time and Frequency Laboratory, Telecommunication Laboratories, No. 12 Lane 551 Ming-Tsu Road Sec. 5, Yang-Mei 326, Taiwan

Received: 23 July 2004 – Revised: 15 December 2004 – Accepted: 10 January 2005 – Published: 30 March 2005

Abstract. We use a digisonde at Jicamarca and a chain of GPS receivers on the west side of South America to investigate the effects of the pre-reversal enhancement (PRE) in $E \times B$ drift, the asymmetry (I_a) of equatorial ionization anomaly (EIA), and the magnetic activity (K_p) on the generation of equatorial spread F (ESF). Results show that the ESF appears frequently in summer (November, December, January, and February) and equinoctial (March, April, September, and October) months, but rarely in winter (May, June, July, and August) months. The seasonal variation in the ESF is associated with those in the PRE $E \times B$ drift and I_a . The larger $E \times B$ drift (>20 m/s) and smaller $|I_a|$ (<0.3) in summer and equinoctial months provide a preferable condition to development the ESF. Conversely, the smaller $E \times B$ drift and larger $|I_a|$ are responsible for the lower ESF occurrence in winter months. Regarding the effects of magnetic activity, the ESF occurrence decreases with increasing K_p in the equinoctial and winter months, but not in the summer months. Furthermore, the larger and smaller $E \times B$ drifts are presented under the quiet ($K_p < 3$) and disturbed ($K_p \geq 3$) conditions, respectively. These results indicate that the suppression in ESF and the decrease in $E \times B$ drifts are mainly caused by the decrease in the eastward electric field.

Keywords. Ionosphere (ionospheric irregularities; equatorial ionosphere)

1 Introduction

Equatorial spread F (ESF) takes its name from the range-dispersed ionogram at stations near the dip equator (Booker and Well, 1938). The ESF usually occurs just after local sunset and the scale sizes of irregularities range from a few centimeters to a few hundred kilometers. Based on the previous investigations, the basic mechanism of ESF onset is the gravitational Rayleigh-Taylor (GRT) instability in conjunc-

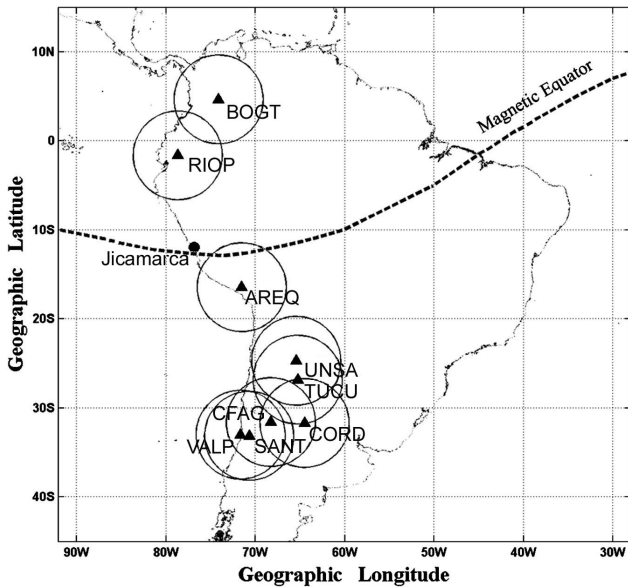
tion with the $E \times B$ drift instability (e.g. Kelley, 1989; Abdu, 2001). The growth rate of instabilities crucially depends on the density gradient that becomes steeper in the nighttime equatorial F-region. Moreover, due to the nonlinear evolution, these instabilities would fully develop into vertically elongated wedges of plasma depletion from bottomside to topside of the F-layer (e.g. Tsunoda et al., 1982; Zalesack et al., 1982; Sultan, 1996).

The ESF studies using ionosonde data (Sales et al., 1996; Stephan et al., 2002; Whalen, 2002), the Global Positioning System (GPS) (Aarons et al., 1996; Mendillo et al., 2000, 2001), radars (Woodman and LaHoz, 1976; Hysell and Burcham, 1998), satellite (Huang et al., 2001; Su et al., 2001), and numerical modeling (Maruyama, 1988; Sultan, 1996) have demonstrated the general morphology of the ESF phenomenon. Now, it is known that there are some candidate mechanisms helping the ESF development. These are (1) the pre-reversal enhancement (PRE) in upward $E \times B$ drift and associated uplifting of the F-layer (Fejer et al., 1999; Whalen, 2002), (2) a small or null transequatorial component of the thermospheric winds and associated symmetry in the equatorial ionization anomaly (EIA) (Maruyama and Matuura, 1984; Maruyama, 1988; Mendillo et al., 2000, 2001), (3) a simultaneous decay of the E region conductivity at both ends of the field line (Tsunoda, 1985; Stephan et al., 2002), and (4) a sharp gradient at the bottomside of the F-layer (Kelley, 1989).

The scope of this paper is to look for the effects of the first and second mechanisms listed above on the ESF onset. For two decades, the earlier works have investigated the variability of $E \times B$ drift on various timescales from day-to-day to season, on longitude, and on solar and geomagnetic activities. Fejer et al. (1979) examined the vertical drift measurements of Jicamarca (12° S, 76.9° W) incoherent scatter radar (ISR) during 1968–1976 to find the associated variations in season and solar cycle. Abdu et al. (1983) pointed out that a necessary condition for the ESF occurrence is the $E \times B$ drift from analysis of Fortaleza (4° S, 38° W) ionosonde data during January–April and September–December in 1978.

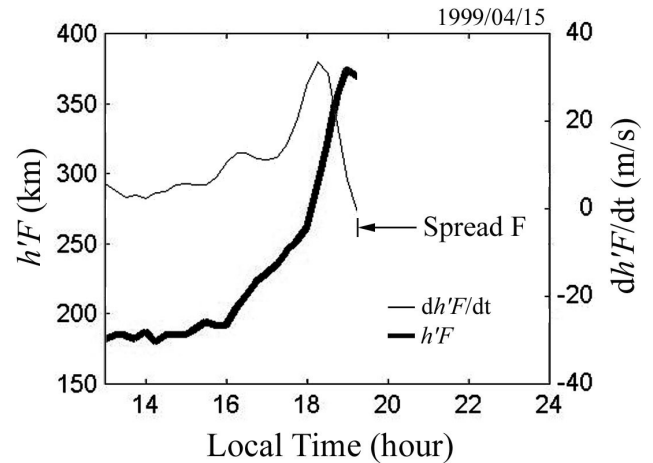
Table 1. The locations of the GPS stations on the west side of South America.

GPS Station	Geographical Latitude	Geographical Longitude	Geomagnetic Latitude
Bogota (BOGT)	4.6° N	74.1° W	16.7° N
Riobamba Permanent Station (RIOP)	1.6° S	78.6° W	10.4° N
Arequipa Laser Station (AREQ)	16.5° S	71.5° W	3.2° S
UNSA Salta (UNSA)	24.7° S	65.4° W	12.2° S
Tucuman (TUCU)	26.8° S	65.2° W	14.3° S
Coronel Fontana (CFAG)	31.6° S	68.2° W	18.4° S
Cordoba (CORD)	31.7° S	64.5° W	18.9° S
Valparaiso Tide Gauge (VALP)	33.0° S	71.6° W	19.6° S
Santiago Tracking Station (SANT)	33.1° S	70.7° W	19.7° S

**Fig. 1.** Map of a digisonde and a chain of nine GPS receivers. The solid dot represents the Jicamarca digisonde, while the triangles symbolize the nine GPS stations on the west side of South America. The circles at each GPS site give the field-of-view for a 400-km intersection height at an elevation angle at 30°.

Recently, Fejer et al. (1999) analyzed the data of the Jicamarca ISR during 1968–1992, and found that the $\mathbf{E} \times \mathbf{B}$ drift and ESF occurrence depend on solar flux, season, and magnetic activity. Whalen (2002) also proposed that the ESF occurrence and $\mathbf{E} \times \mathbf{B}$ drift are a function of magnetic activity and season, using an array of ionospheric sounders in the western American sector during 1958.

Among the studies made on the effects of the second mechanism, most studies employed the short-duration data to explore the day-to-day variability of the meridional wind and associated EIA asymmetry. Maruyama and Matuura (1984) proposed that the asymmetry in the electron density distribution, which is caused by the meridional winds, could suppress the ESF activity. However, they did not show the seasonal variation in the asymmetry in the density distribution.

**Fig. 2.** Sample for $h'F$ (bold line) and $dh'F/dt$ (thin line) on 15 April 1999. The maximum value of $dh'F/dt$ is ~ 32 m/s.

Furthermore, Mendillo et al. (1992) have noted the possible contributions of transequatorial wind in limited samples of ESF day-to-day variability, using an all-sky imaging system at Kwajalen Atoll (9.4° N, 167.5° E). Sastri et al. (1997) applied two ionosondes in Brazil to examine the correlation between the ESF occurrences and the associated meridional winds in June of 1978–1981. Mendillo et al. (2000, 2001) utilized the GPS data near the equinox to calculate the asymmetry of EIA and to test the day-to-day variability of ESF.

In the present paper, we first attempt to investigate the seasonal effect of the EIA asymmetry on the ESF development, besides the seasonal effect of the PRE $\mathbf{E} \times \mathbf{B}$ drift velocity and the magnetic activity. We conducted a one-year observation on the equatorial ionosphere during April 1999–March 2000. A digisonde and a chain of GPS receivers on the west side of South America have been applied to this work. The minimum virtual height of the F-layer ($h'F$) and the latitudinal distribution of the vertical total electron content (VTEC) are used to derive the PRE $\mathbf{E} \times \mathbf{B}$ drift and the asymmetry of EIA, respectively. Further, we utilize these data to study the dependence of ESF on the PRE $\mathbf{E} \times \mathbf{B}$ drift velocity, the asymmetry of EIA, and the magnetic activity (K_p).

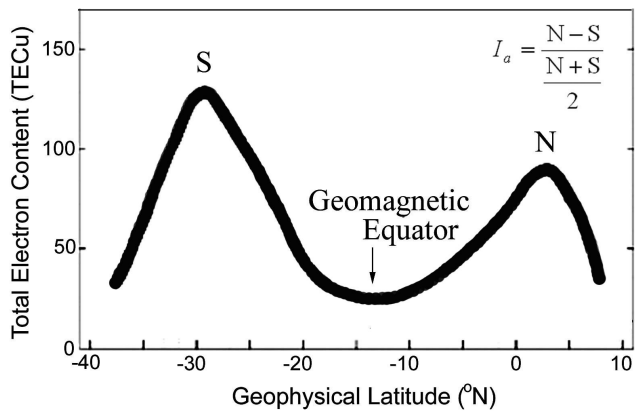


Fig. 3. Schematic illustrating a typical latitudinal distribution of VTEC values. The equation of an asymmetry index I_a of the EIA is represented in the upper-right corner.

2 Experiment setup

Figure 1 shows the locations of a digisonde and all nine GPS receivers. The Jicamarca digisonde (12° S, 76.9° W, geomagnetic latitude: 1.28° N), near the geomagnetic equator, recorded ionograms from April 1999 to March 2000. The presence/absence of ESF and the ionospheric parameters (e.g. $h'F$, $foF2$ – maximum frequency of F-layer) are determined by both the ARTIST program (Reinisch and Haug, 1983; Reinisch, 1996) and manual work. Notably, we focus on the ESF appearing during 18:00–24:00 LT (LT=UT–5 h). The upward PRE velocity is derived by the temporal rate of of $h'F$, $dh'F/dt$, which is described as the $\mathbf{E} \times \mathbf{B}$ drift velocity (Bittencourt and Abdu, 1981). Since the $\mathbf{E} \times \mathbf{B}$ velocity generally reaches its maximum value before the onset of ESF (e.g. Fejer et al., 1999; Whalen, 2002), we apply the maximum value of $dh'F/dt$ between 18:00 LT and the time of ESF onset to the statistical analyses. For example (Fig. 2), as the ESF appears from 19:15 LT on 15 April 1999, the maximum value of $dh'F/dt$, ~ 32 m/s, is adopted in the following studies.

The data of the nine GPS sites (Fig. 1 and Table 1) are retrieved from the International GPS Service (IGS) for Geodynamics. Two of the GPS sites (BOGT and RIOP) are situated north of the geomagnetic equator, and the BOGT site is located near the northern crest of EIA. The other seven GPS receivers (AREQ, UNSA, TUCU, CFAG, CORD, VALP, and SANT) are placed south of the equator. The AREQ is close to the equator, while the TUCU is located near the southern crest. These nine GPS sites offer the equivalent VTEC along the common meridian of $\sim 75^\circ$ W (see Mendillo et al., 2000 for reference). Moreover, an asymmetry index of EIA (I_a), which is related to the transequatorial meridional winds, can be derived from the north versus south crest differences. The I_a is represented as $(N-S)/((N+S)/2)$ (shown in Fig. 3), where N and S are the VTEC values of the north and south crests, respectively (Mendillo et al., 2000). Based on Abdu (2001), the ESF development would depend upon

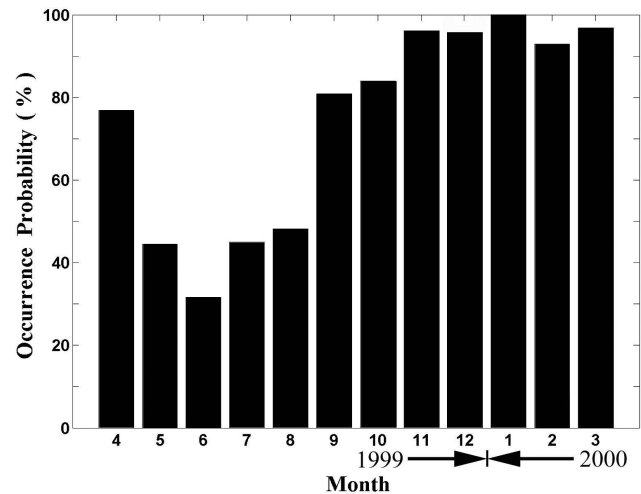


Fig. 4. Seasonal variation in the occurrence probability of ESF during April 1999–March 2000. The highest value (100%) of the occurrence probability appears in January, while the lowest value (30%) is at June.

the symmetry/asymmetry of EIA during the previous 0.5- to 1-h period. Therefore, we examine the I_a between 18:00 LT and the time of ESF onset. While I_a is positive/negative during this period, the maximum/minimum value of I_a is used for the statistical analyses. Notably, I_a is not estimated during December 1999–March 2000, because the BOGT data are not available in these months.

3 Results and discussion

3.1 Seasonal variations in occurrence probability of ESF

Figure 4 displays the seasonal variation in the occurrence probability of ESF. This seasonal variation in the occurrence probability is the percentage of days on which at least one pre-midnight ESF event is observed daily. Clearly, the highest occurrence probabilities (100%) of ESF is in January, near the summer solstice; while the lowest values ($\sim 32\%$) is in June, near the winter solstice. During the equinoctial months (March, April, September, and October), the occurrence probabilities are more than 75%. Generally, the occurrence probability is higher in summer (November, December, January, and February)/equinoctial months than in winter months (May, June, July, and August). In this investigation, the ESF is not categorized into three levels proposed by Whalen (2002), because only one ionosonde is used. Thus, the seasonal variation in ESF (Fig. 4) should be compared with that in the total bottomside spread F (BSSF) of Whalen (2002) (his Fig. 4), who analyzed the ionograms at Huancayo (12° S, 75.3° W) during 1958. Notice that the total BSSF consists of strong and weak BSSF and bubbles (Whalen, 2002), and Huancayo is located at 160 km east of Jicamarca. The comparison result shows that these two

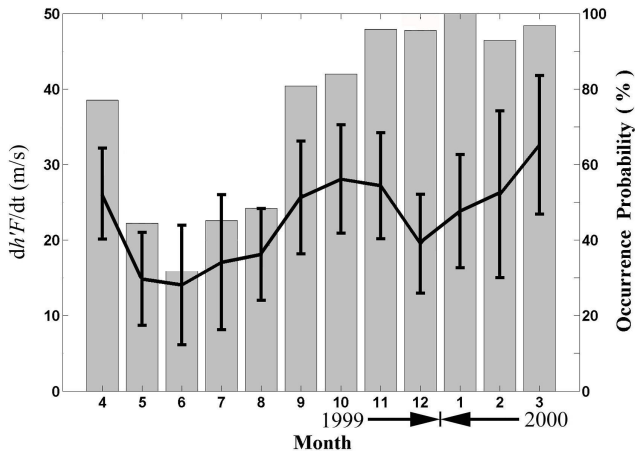


Fig. 5. Seasonal variation in the monthly mean value of the dh'/dt (solid line) and the associated standard deviation (error bar) during April 1999–March 2000. The gray histogram in the background represents the occurrence probability of ESF. Two peak values of dh'/dt appear at October and March, while the smallest value is at June.

seasonal variations are similar: the highest and lowest occurrence probabilities are in summer and winter, respectively.

3.2 Seasonal variations in the PRE $E \times B$ drift

We examine the seasonal variation in the PRE $E \times B$ drift by deriving the monthly mean value of dh'/dt . Figure 5 shows the seasonal variation in the monthly mean value of dh'/dt (solid line) and the associated standard deviation (error bar), as well as the occurrence probability of ESF (gray histogram in background). It is apparent that two peak values, ~ 28 and ~ 32 m/s, appear in October and March, respectively; while the smallest dh'/dt , ~ 14 m/s, is in June. The seasonal variation in dh'/dt is close to Fejer et al. (1999), who propounded that the largest and smallest vertical drift velocities are at the equinox and the June solstices, respectively. Consequently, the mean dh'/dt are ~ 14 – 18 and ~ 20 – 27 m/s during May–August and November–February, respectively. These mean values are also close to Fejer et al. (1999), in which the maximum values are ~ 18 and ~ 28 – 34 m/s, respectively, in May–August and November–February, during a high solar activity period. However, in March, April, September, and October, the values of ~ 25 – 32 m/s are slightly smaller than the maximum value (~ 33 – 48 m/s) of Fejer et al. (1999) during a high solar activity period.

In the equinoctial months, the larger dh'/dt is associated with the higher ESF occurrence. This demonstrates that the larger upward drift lifts the F-layer to higher altitudes, which not only results in favorable conditions for the GRT instability but the larger eastward electric field itself causes an $E \times B$ drift instability (Maruyama, 1988; Kelley, 1989). In contrast, the small dh'/dt in the winter months would not raise the F-layer to altitudes where it is high enough to generate irregularities. Thus, the ESF occurrences are lower in the

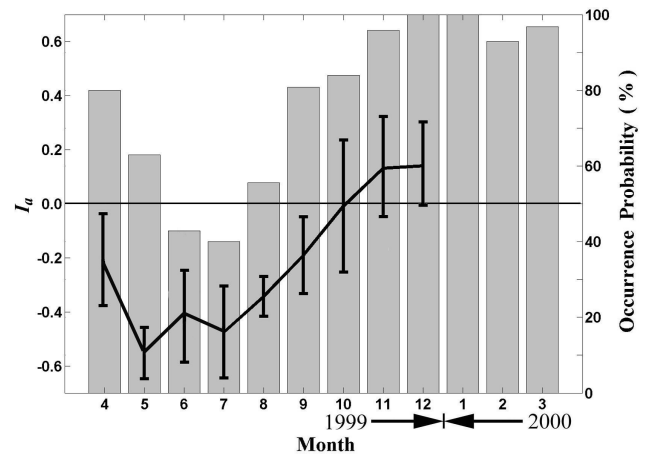


Fig. 6. Seasonal variation in the monthly mean value of I_a (solid line) and the associated standard deviation (error bar) during April 1999–March 2000. The gray histogram in the background represents the occurrence probability of ESF. Notice that I_a is not estimated during December 1999–March 2000, because the GPS data of BOGT are not available in these months.

winter months. These results reveal that the PRE $E \times B$ drift plays an important role as the seeding mechanism of ESF development (Sultan, 1996; Fejer et al., 1999; Kudeki and Bhattacharyya, 1999; Whalen, 2002). Additionally, there are also other seeding mechanisms such as gravity waves (Sultan, 1996; Kudeki and Bhattacharyya, 1999).

During the summer months, the mean values of dh'/dt , ~ 20 – 27 m/s, are smaller than that at the equinox, but higher than that in the winter. Notice that the occurrence probability of ESF in January is the highest value (100%) between April 1999 and March 2000. Such kind of correlation between the dh'/dt and the ESF occurrence indicates that there would be another mechanism to help the ESF development, besides the larger upward velocity. According to Maruyama (1988) and Fejer et al. (1999), the late reversal time of upward drift should be a considerable reason for the highest occurrence probability at December solstice.

3.3 Seasonal variations in the asymmetry of EIA

Figure 6 shows the seasonal variation in the monthly mean value of I_a (solid line), the associated standard deviation (error bar), and the occurrence probability of ESF (gray histogram in background). It is found that I_a is negative and $|I_a|$ is greater than 0.3 during May–August (winter months). In April, September, and October (equinoctial months), I_a is also negative, but $|I_a|$ is smaller than 0.3. In contrast, I_a is positive and $|I_a|$ is smaller than 0.3 in November (summer months). According to Mendillo et al. (2000, 2001), the I_a index is associated with the transequatorial meridional winds that would distort a presumed symmetrical EIA. Thus, the meridional winds are generally southward and northward in April–October and November, respectively. Moreover, the greater values (>0.3) of $|I_a|$ during May–August indicate

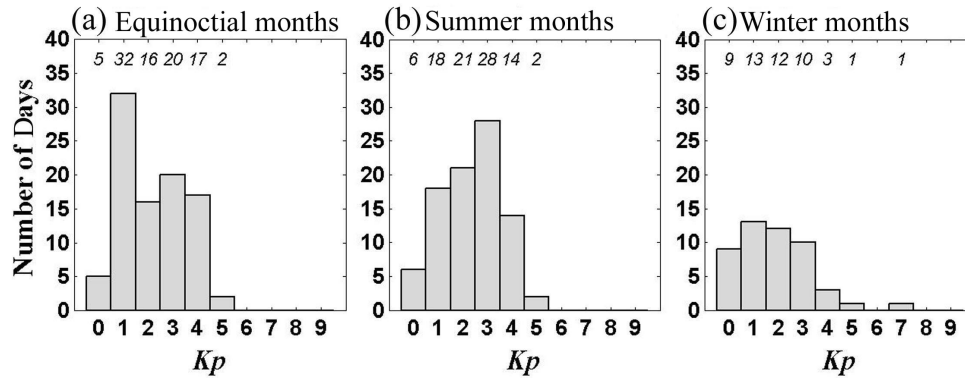


Fig. 7. Occurrence of ESF on each day for each of the equinoctial (a), summer (b), and winter (c) months plotted as a function of K_p determined as the average during the 6 h prior to measurement.

that the associated meridional winds in the winter months are stronger than that in the equinoctial (April, September, and October) and summer (November) months. These are similar to the meridional winds used by Maruyama (1988), in which the wind is northward and stronger near the winter solstice (in his Fig. 3).

As shown in Fig. 6, the greater $|I_a|$ and lower ESF occurrence concurrently appear during May–August. Based on Maruyama and Matuura (1984), Maruyama (1988), and Mendillo et al. (1992), this negative correlation between these two parameters indicates that the asymmetric EIA is related to the inhibition of ESF development. This is because the asymmetry of EIA would form an asymmetry in distribution of conductivity and recombination rates along the field line. Then, the asymmetry in conductivity and recombination rates further suppresses the GRT growth rate (Maruyama and Matuura, 1984; Maruyama, 1988; Mendillo et al., 1992). Besides the suppressive effect of I_a , the smaller dh'/dt in the winter months (Fig. 5) is not helpful in developing the ESF either. Therefore, the lower ESF occurrence is caused by the greater $|I_a|$ and the smaller dh'/dt .

On the other hand, the smaller $|I_a|$ and higher ESF occurrence concurrently appear in April, September, and October. This result shows that the $|I_a|$ is negatively correlated with the ESF occurrence, and demonstrates that the asymmetry in conductivity and recombination rates would be not strong enough to suppress the GRT growth rate. Recall that, in the equinoctial months (Fig. 5), the values of dh'/dt are larger. Thus, the higher ESF occurrence is due to not only the larger dh'/dt but also the smaller $|I_a|$ during the equinoctial months. Additionally, the smaller $|I_a|$ and higher ESF occurrence are also seen simultaneously in November. Similar to the equinoctial months, the higher ESF occurrence is caused by both the smaller $|I_a|$ and larger dh'/dt .

3.4 Dependence on the magnetic activity (K_p)

The ESF is examined on each day in relation to the magnetic activity on that day, which is taken as the average value of K_p recorded during the 6 h prior to the onset of ESF (e.g.

Fejer et al., 1999; Whalen, 2002). Notice that the average K_p is generally derived from the interval of 18:00–24:00 UT (13:00–19:00 LT).

The number of days on ESF are organized by season and plotted versus the average K_p in Fig. 7. For the equinoctial months (Fig. 7a), the ESF occurs frequently and rarely when K_p is 1 and 5, respectively. Except $K_p=2$, the number of days tends to decrease with increasing K_p in the equinoctial months. Moreover, a descending trend from $K_p=1$ to 5 is obvious in the winter months (Fig. 7c), but not in the summer months (Fig. 7b). The decreasing trends in the equinoctial and winter months indicate that the increasing magnetic activity progressively suppresses the ESF generation in these two seasons (Fejer et al., 1999; Whalen, 2002). However, these distributions are not consistent with that of total BSSF in Whalen (2002) (his Fig. 5), which reported that the decreasing trends existed in the equinoctial and summer months, not in the winter months. This might be because the distribution of K_p days is different for each seasons between 1958 and 1999–2000.

To further reveal the geomagnetic effect on dh'/dt and I_a , we examine the monthly mean values of dh'/dt (Fig. 8a) and I_a (Fig. 8b) under quiet ($K_p < 3$) and disturbed ($K_p \geq 3$) conditions during April 1999–March 2000. In the equinoctial months, the mean dh'/dt as $K_p \geq 3$ is less than that as $K_p < 3$, and the differences are ~ 3 – 8 m/s. For the summer months, dh'/dt is larger under the quiet condition and the differences are ~ 2 – 5 m/s, except February. Furthermore, for the winter months, dh'/dt as $K_p < 3$ is also larger in May and August, and the differences are ~ 8 and ~ 3 m/s, respectively. Notice that no dh'/dt as $K_p \geq 3$ is shown in June, because all K_p are smaller than 3. Furthermore, only one dh'/dt as $K_p \geq 3$ is in July, and this large upward velocity is related to the prompt penetration effect (Fejer and Scherliess, 1997; Fejer et al., 1999). Generally, the dh'/dt is smaller under the disturbed condition, and these results are similar to Fejer et al. (1999), who proposed that the maximum vertical drift is, respectively, larger and smaller under the quiet and disturbed conditions during a high solar activity period (their Fig. 7). The decrease in dh'/dt indicates that the maximum

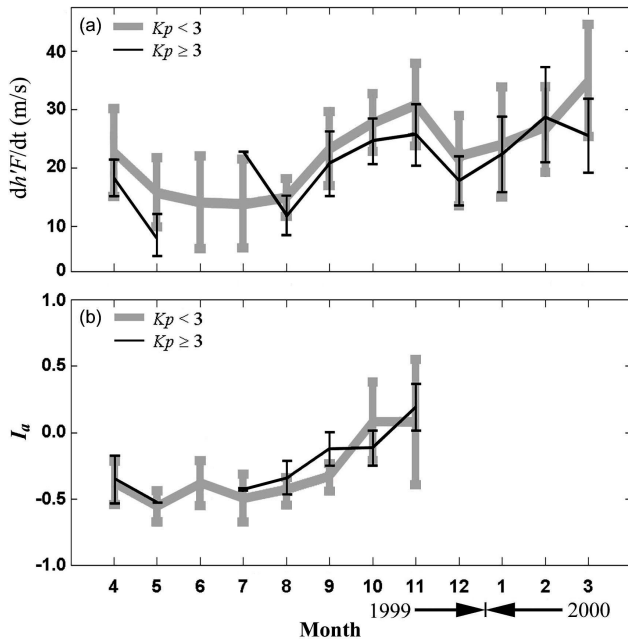


Fig. 8. Seasonal variations of the monthly mean values of $dh/F/dt$ (a) and I_a (b) between April 1999 and March 2000. The black thin and gray bold lines represent the mean values under the disturbed ($K_p \geq 3$) and quiet ($K_p < 3$) conditions, respectively. The error bars are the associated standard deviation.

eastward electric field of PRE is reduced by the disturbed magnetic activity (Scherliess and Fejer, 1997). Moreover, this decrease is due to the disturbance dynamo electric fields which decrease the upward drift velocity near sunset (Fejer et al., 1999).

Regarding the I_a (Fig. 8b), it is found that the mean $|I_a|$ as $K_p < 3$ is larger than that as $K_p \geq 3$ in August and September. In contrast, the mean $|I_a|$ as $K_p < 3$ is smaller than that as $K_p \geq 3$ in October and November. Moreover, the mean $|I_a|$ is nearly the same between the quiet and disturbed conditions in April, May, and July. These results suggest that the effect of the magnetic activity on I_a seems not to be evident. Since the I_a is related to the meridional winds, the disturbed magnetic activity does not obviously affect the strength of the winds.

4 Summary and conclusion

We have analyzed the ionogram and TEC data to investigate the long-duration effects of the PRE $\mathbf{E} \times \mathbf{B}$ drift, the EIA asymmetry, and the magnetic activity on the ESF generation. The ionogram and TEC data during April 1999–March 2000 are obtained by a digisonde and a chain of GPS receivers, respectively. It is remarkable that this work is a first attempt to examine the seasonal variation in the EIA asymmetry. The results point out that the dependence of ESF on season and magnetic activity can be explained by the corresponding effects on the $\mathbf{E} \times \mathbf{B}$ drift and EIA asymmetry.

For the seasonal variation, the ESF appears frequently in the summer and equinoctial months, but rarely in the

winter months. Such kind of occurrence variation is evidently correlated to the magnitude of $\mathbf{E} \times \mathbf{B}$ drift. The correlations in summer and equinoctial months demonstrate that the ionosphere is lifted to higher altitudes where the gravitational drift term is dominant in the GRT growth rate, leading to the development of the ESF, when the upward drift velocities are larger than 20 m/s. Moreover, the influence of the EIA asymmetry (I_a) is also significant regarding the ESF occurrence. The value of $|I_a|$ is generally anti-correlated to the ESF occurrence. This anti-correlation indicates that the EIA asymmetry ($|I_a| > 0.3$) could suppress the GRT growth rate, because of the asymmetry in distribution of conductivity and recombination rates.

For the magnetic activity, we have shown that the number of ESF days decreases with increasing K_p in the equinoctial and winter months, but not in the summer months. This descending trend suggests that the magnetic activity progressively suppresses the ESF generation in those two months. Additionally, our results show that the $\mathbf{E} \times \mathbf{B}$ velocity is larger and smaller under the quiet and disturbed conditions, respectively. This indicates that this ESF suppression would be due to the effect of the magnetic activity on the $\mathbf{E} \times \mathbf{B}$ velocity. Contrarily, it is found that I_a is not obviously related to the magnetic activity.

Acknowledgements. This work is supported by the grant of National Science Council: NSC 93-2119-M-231-002 and NSC 93-2111-M-008-022-AP5. The authors would like to thank the International GPS Service (IGS) for Geodynamics for GPS data and to the World Data Center for Geomagnetism in Kyoto for providing K_p data.

Topical Editor M. Lester thanks a referee for his/her help in evaluating this paper.

References

- Aarons, J., Mendillo, M., and Yantosca, R.: GPS phase fluctuations in the equatorial region during the MISETA 1994 campaign, *J. Geophys. Res.*, 101, 26 851–26 862, 1996.
- Abdu, M. A.: Outstanding problems in the equatorial ionosphere-thermosphere electrodynamics relevant to spread F, *J. Atmos. Solar-Terr. Phys.*, 63, 869–884, 2001.
- Abdu, M. A., de Medeiros, R. T., Bittencourt, J. A., and Batista, I. S.: Vertical ionization drift velocities and range type spread in the evening equatorial ionosphere, *J. Geophys. Res.*, 88, 399–402, 1983.
- Bittencourt, J. A. and Abdu, M. A.: A theoretical comparison between apparent and real vertical ionization drift velocities in the equatorial F-region, *J. Geophys. Res.*, 86, 2451–2454, 1981.
- Booker, H. G. and Wells, H. W.: Scattering of radio waves by the F-region of the ionosphere, *J. Geophys. Res.*, 43, 249–256, 1938.
- Fejer, B. G. and Scherliess, L.: Empirical models of storm time equatorial zonal electric fields, *J. Geophys. Res.*, 102, 24 047–24 056, 1997.
- Fejer, B. G., Farley, D. T., Woodman, R. F., and Calderon, C.: Dependence of equatorial F-region vertical drifts on season and solar cycle, *J. Geophys. Res.*, 84, 5792–5796, 1979.

- Fejer, B. G., Scherliess, L., and de Paula, E. R.: Effects of the vertical plasma drift velocity on the generation and evolution of equatorial F, *J. Geophys. Res.*, 104, 19 859–19 869, 1999.
- Huang, C. Y., Burke, W. J., Machuzak, J. S., Gentile, L. C., and Sultan, P. J.: DMSP observations of equatorial plasma bubbles in the topside ionosphere near solar maximum, *J. Geophys. Res.*, 106, 8131–8142, 2001.
- Hysell, D. L. and Burcham, J. D.: JULIA radar studies of equatorial spread F, *J. Geophys. Res.*, 103, 29 155–29 167, 1998.
- Kelley, M. C.: The Earth's Ionosphere, *Int. Geophys. Ser.*, Academic, San Diego, Calif., 43, 1989.
- Kudeki, E. and Bhattacharyya, S.: Post sunset vortices in equatorial F-region plasma drifts and implications for bottomside spread F, *J. Geophys. Res.*, 104, 28 163–28 170, 1999.
- Maruyama, T.: A diagnostic model for equatorial spread F 1. model description and application to electric field and neutral wind effects, *J. Geophys. Res.*, 93, 14 611–14 622, 1988.
- Maruyama, T. and Matuura, N.: Longitudinal variability of annular changes in activity of equatorial spread F and plasma depletions, *J. Geophys. Res.*, 89, 10 903–10 912, 1984.
- Mendillo, M., Baumgardner, J., Pi, X., and Sultan, P. J.: Onset conditions for equatorial spread F, *J. Geophys. Res.*, 97, 13 865–13 876, 1992.
- Mendillo, M., Lin, B., and Aarons, J.: The application of GPS observation to equatorial aeronomy, *Radio Sci.*, 35, 885–904, 2000.
- Mendillo, M., Meriwether, J., and Miodni, M.: Testing the thermospheric neutral wind suppression mechanism for day-to-day variability of equatorial F, *J. Geophys. Res.*, 106, 3655–3663, 2001.
- Reinisch, B. W.: Modern ionosondes, in: *Modern Radio Science*, edited by: Kohl, H., Ruester, R., and Schlegel, K., European Geophysical Society, Katlenburg-Lindau, Germany, 440–458, 1996.
- Reinisch, B. W. and Haug, X.: Automatic calculation of electron density profiles from digital ionograms, 3. Processing of bottomside ionograms, *Radio Sci.*, 18, 477–492, 1983.
- Sales, G. S., Reinisch, B. W., Scali, J. L., Dozois, C., Bullett, T. W., Weber, E. J., and Ning, P.: Spread-F and the structure of equatorial ionization depletions in the Southern Anomaly Region, *J. Geophys. Res.*, 101, 26 819–26 827, 1996.
- Sastri, J. H., Abdu, M. A., Batista, I. S., and Sobral, H. A.: Onset conditions of equatorial (range) spread F at Fortaleza, Brazil, during the Jun solstice, *J. Geophys. Res.*, 102, 24 013–24 021, 1997.
- Scherliess, L. and Fejer, G. B.: Storm time dependence of equatorial disturbance dynamo zonal electric fields, *J. Geophys. Res.*, 102, 24 037–24 046, 1997.
- Stephan, A. W., Colerico, M., Mendillo, M., Reinisch, B. W., and Anderson, D.: Suppression of equatorial spread F by sporadic E, *J. Geophys. Res.*, 107 (A2), doi:10.1029/2001JA000162, 2002.
- Su, S. Y., Yeh, H. C., and Heelis, R. A.: ROCSAT-1 IPEI observations of equatorial spread F—some early transitional scale results, *J. Geophys. Res.*, 106, 29 153–29 159, 2001.
- Sultan, P. J.: Linear theory and modeling of the Rayleigh-Taylor instability leading to the occurrence of equatorial F, *J. Geophys. Res.*, 101, 26 875–26 891, 1996.
- Tsunoda, R.: Control of the seasonal and longitudinal occurrence of equatorial scintillations by the longitudinal gradient in the integrated E region Pedersen conductivity, *J. Geophys. Res.*, 90, 447–456, 1985.
- Tsunoda, R. T., Livingston, R. C., McClure, J. P., and Hanson, W. B.: Equatorial plasma bubbles: Vertical elongated wedges from the bottomside F-layer, *J. Geophys. Res.*, 87, 9171–9180, 1982.
- Whalen, J. A.: Dependence of the equatorial bubbles and bottomside spread F on season, magnetic activity, and $E \times B$ drift velocity during solar maximum, *J. Geophys. Res.*, 107 (A2), doi:10.1029/2001JA000039, 2002.
- Woodman, R. F. and LaHoz, C.: Radar observation of F-region equatorial irregularities, *J. Geophys. Res.*, 81, 5447–5466, 1976.
- Zalesack, S. T., Ossalow, S. L., and Chaturvedi, P. K.: Nonlinear equatorial spread F: the effect of neutral winds and background Pederson conductivity, *J. Geophys. Res.*, 87, 151–166, 1982.